



HAL
open science

Dynamical behavior of damaged railway sleeper subjected to moving loads: Parametric study of crack properties

Thuy-Duong Le, Le-Hung Tran

► **To cite this version:**

Thuy-Duong Le, Le-Hung Tran. Dynamical behavior of damaged railway sleeper subjected to moving loads: Parametric study of crack properties. Vietnam Journal of Mechanics, 2025, pp.28. 10.15625/0866-7136/21542 . hal-04894600

HAL Id: hal-04894600

<https://hal.science/hal-04894600v1>

Submitted on 17 Jan 2025

HAL is a multi-disciplinary open access archive for the deposit and dissemination of scientific research documents, whether they are published or not. The documents may come from teaching and research institutions in France or abroad, or from public or private research centers.

L'archive ouverte pluridisciplinaire **HAL**, est destinée au dépôt et à la diffusion de documents scientifiques de niveau recherche, publiés ou non, émanant des établissements d'enseignement et de recherche français ou étrangers, des laboratoires publics ou privés.

DYNAMICAL BEHAVIOR OF DAMAGED RAILWAY SLEEPER SUBJECTED TO MOVING LOADS: PARAMETRIC STUDY OF CRACK PROPERTIES

Thuy-Duong Le^{1,*}, Le-Hung Tran²

¹*Faculty of Civil Engineering, VNU University of Engineering and Technology,
144 Xuan Thuy street, Hanoi, 100000, Vietnam*

²*EMGCU/MAST, Université Gustave Eiffel, 14-20 boulevard Newton,
Champs-sur-Marne, 77420, France*

*E-mail: lethuyduong@vnu.edu.vn

Received: 16 September 2024 / Revised: 25 December 2024 / Accepted: 02 January 2025

Published online: 07 January 2025

Abstract. This study investigates the dynamic responses of cracked beams placed on a visco-elastic foundation and subjected to moving loads. Utilizing the Euler–Bernoulli beam model, the behavior of the beams is characterized, accounting for multiple open cracks on one side with varying depths. Through the application of Fourier transform techniques and Green’s function, the dynamic response of the beam is analytically determined in the frequency domain. Furthermore, an analytical model for railway sleepers is developed by integrating them with a periodically supported beam model. This integrated model enables efficient computation of the dynamic behavior of damaged sleepers, where cracks are present at specific locations. Additionally, a calculation model utilizing the finite element method is established and compared with the analytical model. The parametric study shows the influence of crack properties on the dynamic beam responses.

Keywords: cracked beam, railway sleeper, visco-elastic foundation, Euler–Bernoulli beam.

1. INTRODUCTION

Soil-structure interaction, as seen in pipelines, footings, piles, and railways, often employs simplified one-dimensional (1D) beam models due to their straightforward geometry. The ground is frequently modeled by using Winkler [1], Pasternak [2], Vlasov [3], or Kerr [4] foundations. This study adopts the Kelvin–Voigt model to simulate the interaction between a beam and its foundation in both static and dynamic settings. Unlike

the simpler Winkler model, the Kelvin–Voigt model introduces a damping term, making it more suitable for capturing the dynamic behavior of the beam–foundation system. Euler–Bernoulli beam theory is typically employed to describe vertical displacements resulting from transversely distributed forces.

The dynamic response of a beam on an elastic foundation can be studied through analytical, numerical, or semi-analytical methods. The Euler–Bernoulli and Timoshenko beam theories are commonly used in these analyses. Past research has extensively examined the vibration of beams supported on Kelvin–Voigt foundations, including works on the stabilization and eigenfrequency effects. Recent studies have also focused on the impact of localized damping and size-dependent foundation properties. Zhang et al. [5] focus on the spectrum of the Euler–Bernoulli beam equation with Kelvin–Voigt damping. Later, a logarithmic stabilization of the Euler–Bernoulli transmission plate equation with locally distributed Kelvin–Voigt damping is presented by Hassine et al. [6]. Recently, a nonlinear vibration of a fractional Kelvin–Voigt visco-elastic beam on a nonlinear elastic foundation is presented by Javadi et al. [7]. The responses of the beam–soil system are also developed by using the theory of the Timoshenko beam. Vibration of a non-local Kelvin–Voigt visco-elastic damped Timoshenko beam is developed by Lei et al. [8]. The effect of local Kelvin–Voigt damping of eigenfrequencies of twisted Timoshenko beams is investigated by Chen et al. [9–12] in several scientific works. Recent works focus on the influence of the size-dependent foundation on the beam responses. Zhang et al. [13, 14] studied the buckling and free vibration of functionally graded (FG) sandwich Timoshenko beams resting on a non-local visco-elastic foundation.

In particular, based on a beam–soil model, numerous works have been developed in the railway engineering domain. [15] studied the vibration of solids and structures under a moving load. Nguyen and Duhamel [16, 17] presented a finite element procedure for nonlinear structures in moving coordinates. The dynamics of beams on non-uniform nonlinear foundations subjected to moving loads are calculated by [18]. The dynamic model of railway sleepers on a Kelvin–Voigt foundation is developed by Tran et al. [19–25].

Besides the studies of an undamaged beam which includes all those mentioned above, it should be noted that the presence of cracks in buried or ground-supported structures is not infrequent [26, 27]. The flexibility of the system increases when the cracks appear locally. The responses of damaged structures are obviously changed and consequently, the system eventually fails. Therefore, the dynamic behavior of the damaged beam–soil system is a subject of undeniable technological interest. In the existing works, the cracked beam is commonly considered as a set of segments connected by massless rotational springs which are located at the crack positions. This approach has been investigated in numerous researches [28, 29]. The stiffness of a rotational spring is

determined as a function of crack length with the help of Linear Elastic Fracture Mechanics theory (see also Lemaitre [30]). By using this model, Khiem et al. [31] worked on a simplified method to calculate the natural frequency of a multiply-cracked beam. Later, Lele et al. [32] modeled a transverse vibration of a short beam for crack detection and modeled the crack extension by using FEM. Viola et al. [33] developed a method to detect the crack location by using the cracked beam element method. A continuous model for the transverse vibration of cracked Timoshenko beams is presented by Carneiro [34]. Hearndon [35] described a non-destructive damage detection method using an effective modulus approach. A vibration of a cracked beam on an elastic foundation is analyzed by Batihan [36]. By introducing rotational and longitudinal springs which result in the slope and transverse displacement discontinuities at the cracked cross-sections, Darban et al. [37] calculated the free transverse vibrations of nano-beams. Recently, the natural frequencies of the vibration of a cracked rectangular Timoshenko beam within an elastic medium have been calculated by Loya et al. [38, 39]. For a system consisting of a cracked beam and soil subjected to moving loads, Pham et al. [40] calculated the dynamic response of a cracked multi-span continuous beam subjected to a moving multi-axle vehicle load. Yan et al. [41] calculated the dynamic behavior of edge-cracked shear deformable FG beams on an elastic foundation under a moving load. Several methods have been developed in recent years to model cracks in structures and materials. Rezaiee et al. [42] used a numerical method to develop a force-based rectangular cracked element, while Zheng et al. [43] employed a phase field fracture method to model a hyper-elastic material and hydro-gel using the ABAQUS software.

This study focuses on calculating the dynamic responses of a cracked beam on a Kelvin–Voigt foundation subjected to moving loads using an Euler–Bernoulli beam model. Open cracks on one side of the beam are modeled as rotational springs, with stiffness dependent on crack depth. Analysis is performed in the frequency domain using Green’s function. A Finite Element Method (FEM) model, developed with Cast3M software, includes a structural system of rails, sleepers, an elastic foundation, and connecting springs. Dynamic computations are conducted using FEM and compared with analytical solutions. Additionally, a dynamic model of railway sleepers integrating periodically supported beam and cracked beam models is presented. Numerical and analytical results are discussed in Section 3, followed by concluding remarks in Section 4.

2. THEORY

2.1. Dynamic model for the railway sleeper

On this track, the Euler–Bernoulli beam model is used to illustrate the dynamic behaviors of the sleepers. The sleeper with a total length of $2L$ with $(-L \leq x \leq L)$ is placed

on a viscoelastic foundation modeled by a Kelvin–Voigt foundation as shown in Fig. 1 and subjected to the two moving loads and on rails 1 and 2, respectively.

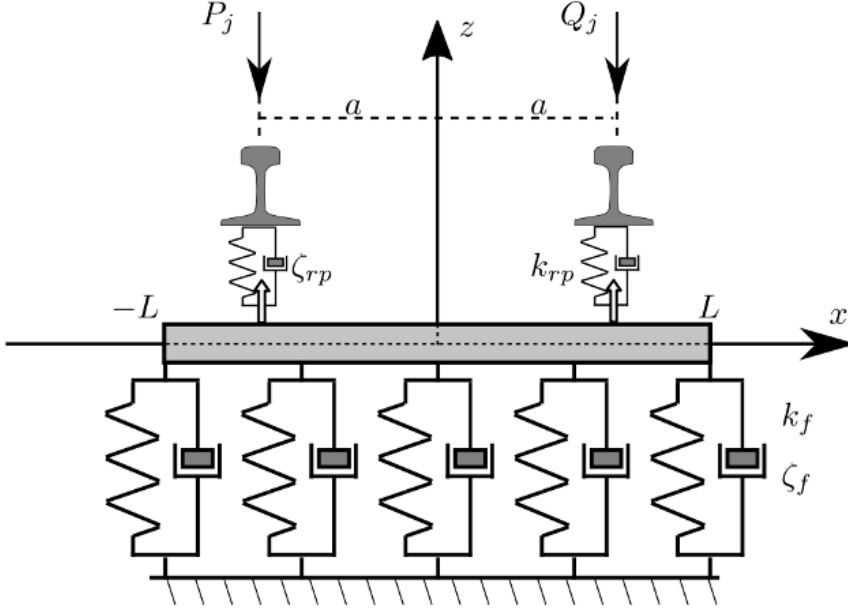


Fig. 1. Analytical model representation for the railway sleeper

It should be noted that P_j and Q_j are the wheel loads acting on the rails while R_1 and R_2 are the reaction forces from the supports acting back on the rails. These two forces are different because the wheel loads act on the rails and are distributed to the supports. In the time domain, the dynamic vertical displacement of the beam is written as follows:

$$B_s \frac{\partial^4 w_s}{\partial x^4} + M_s \frac{\partial^2 w_s}{\partial t^2} + k_f w_s + \zeta_f \frac{\partial w_s}{\partial t} = F(x, t), \quad (1)$$

where k_f is stiffness, ζ_f is damping coefficient, $B_s = E_s I_s$ is flexural rigidity, $M_s = \rho_s S_s$ is mass per length unit.

Two reaction forces $R_1(t)$ and $R_2(t)$ apply on a sleeper from the rail through a rail pad that is considered to act as dampers and springs. The sleeper is subjected to a total force at two rail positions $\pm a$ which can be written using Dirac's delta distribution as follows:

$$F(x, t) = -R_1(t)\delta(x - a) - R_2(t)\delta(x + a), \quad (2)$$

where the total force in the frequency domain can be expressed as follows:

$$\hat{F}(x, \omega) = -\hat{R}_1(\omega)\delta(x - a) - \hat{R}_2(\omega)\delta(x + a).$$

Through the utilization of Fourier's transform and the inclusion of Eq. (2), Eq. (1) can be expressed in the frequency domain as follows:

$$\frac{\partial^4 \hat{w}_s(x, \omega)}{\partial x^4} - \frac{M_s \omega^2 - k_b}{B_s} \hat{w}_s(x, \omega) = -\frac{\hat{R}_1(\omega)}{B_s} \delta(x - a) - \frac{\hat{R}_2(\omega)}{B_s} \delta(x + a), \quad (3)$$

where $\hat{w}_s(x, \omega)$ is the displacement of the beam in the frequency domain and the stiffness dynamic of the foundation k_b is defined as: $k_b = k_f + j\omega\zeta_f$.

Eq. (3) outlines the beam responses. To solve this equation, we will employ Green's function, determined as follows:

$$\frac{\partial^4 G(x, \omega; a)}{\partial x^4} - \lambda_s^4 G(x, \omega; a) = \delta(x - a).$$

The dynamic equation of the railway sleeper subjected to the two moving loads is obtained where the solutions are presented in Appendix A. Moreover, it can be considered that the n open cracks on one side of the beam appear in the interval between the two rails ($-a < x_{c_j} < a$). Therefore, two Green's functions $G(x, \omega; \pm a)$ are calculated using Eq. (A.4) which is explained in Appendix A.

2.2. Dynamic model for the rail

The railway route depicted in Fig. 2 can be segmented into two distinct models: one for the rail, depicted as a regularly supported beam, and the other for the sleeper, illustrated as a beam positioned on a visco-elastic foundation. Combining these two models results in dynamic track responses.

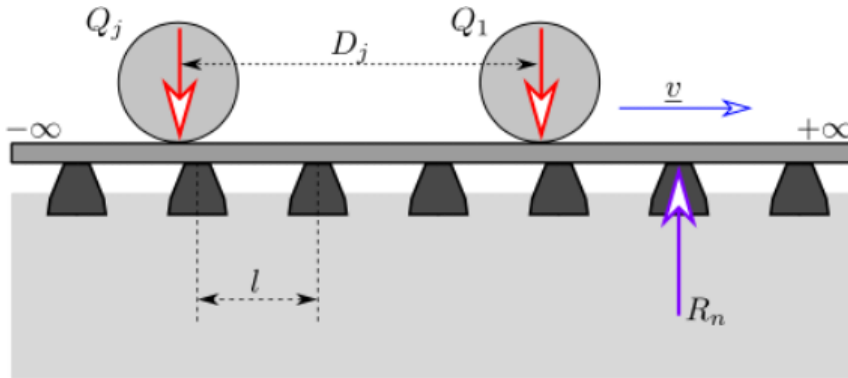


Fig. 2. Ballasted railway track

In this model, the rails are conceptualized as infinite beams positioned on the periodic supports and exposed to K moving loads Q_j characterized by the speed ν and distance D_j from the first wheel as shown in Fig. 3.

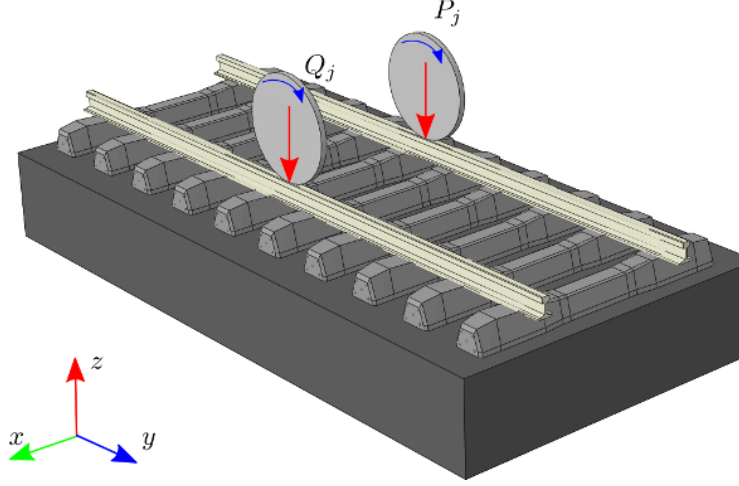


Fig. 3. Periodically supported beam under the influence of moving loads

Let $R_n(t)$ represent the reaction forces of the supports on the rail and $w_r(y, t)$ the displacement of the rail in the time domain. The dynamic behavior of the rail is described using the Euler–Bernoulli beam model as follows:

$$B_r \frac{\partial^4 w_r}{\partial y^4} + M_r \frac{\partial^2 w_r}{\partial t^2} + \sum_{n=-\infty}^{\infty} R_n(t) \delta(y - nl) = \sum_{j=1}^K Q_j \delta(y + D_j - vt),$$

where $B_r = E_r I_r$ is the flexural rigidity; $M_r = \rho_r S_r$ is the mass per length unit and l is the distance between two supports. In the steady-state condition, it is considered that the responses of the supports are the same function with a time delay, for moving from one support to the next one (Floquet's theorem): $R_n(t) = R\left(t - \frac{nl}{v}\right)$. Therefore, using the Fourier transform of the last equation two times and then the inverse Fourier transform, the relationship between the reaction force and the displacement of the support in the frequency domain can be written as follows:

$$\hat{R}(\omega) = \mathcal{K}(\omega) \hat{w}_r(0, \omega) + \mathcal{Q}(\omega), \quad (4)$$

where the two functions $\mathcal{K}(\omega)$ and $\mathcal{Q}(\omega)$ are defined as follows:

$$\begin{cases} \mathcal{K}(\omega) = 4\lambda_r B_r \left[\frac{\sin l\chi_r}{\cos l\chi_r - \cos \frac{\omega l}{v}} - \frac{\sinh l\chi_r}{\cosh l\chi_r - \cos \frac{\omega l}{v}} \right]^{-1}, \\ \mathcal{Q}(\omega) = \frac{\mathcal{K}(\omega)}{\nu B_r \left(\left(\frac{\omega}{v} \right)^4 - \chi_r^4 \right)} \sum_{j=1}^K Q_j e^{-j \frac{\omega D_j}{v}}, \end{cases}$$

where $\chi_r = \sqrt[4]{\frac{M_r \omega^2}{B_r}}$. Each support can be considered as a spring in the frequency domain with the stiffness \mathcal{K} . This relationship depends only on the rail and moving load parameters, hence it holds for all types of foundations.

2.3. Coupling of the two models and solution

The beam displacement can be computed using the Green's function as follows:

$$\hat{w}_s(x, \omega) = -\hat{R}(\omega)G(x, \omega; a). \quad (5)$$

Therefore, the displacement of the railway sleeper subjected to the two reaction forces can be defined as follows:

$$\begin{cases} \hat{w}_s(a, \omega) = -\hat{R}_1(\omega)G(a, \omega; a) - \hat{R}_2(\omega)G(a, \omega; -a), \\ \hat{w}_s(-a, \omega) = -\hat{R}_1(\omega)G(-a, \omega; a) - \hat{R}_2(\omega)G(-a, \omega; -a). \end{cases} \quad (6)$$

In this model, the rail-pad can be considered as a spring-damper system. In the frequency domain, the reaction force can be calculated via the rail-pad as follows:

$$\begin{cases} \hat{R}_1(\omega) = k_p(\omega)(\hat{w}_1(\omega) - \hat{w}_s(a, \omega)), \\ \hat{R}_2(\omega) = k_p(\omega)(\hat{w}_2(\omega) - \hat{w}_s(-a, \omega)), \end{cases}$$

where $\hat{w}_1(\omega)$ and $\hat{w}_2(\omega)$ are the displacements of rails 1 and 2 at the crossing points with the reference sleeper ($y = 0$ and $x = \pm a$), $k_p = k_{rp} + j\omega\zeta_{rp}$ is the dynamic stiffness of the rail pad. By substituting the last result into Eq. (4), the relationship between the reaction force put on the sleeper and the sleeper displacement is given as follows:

$$\begin{cases} \hat{R}_1(\omega) = \frac{k_p \mathcal{K}}{k_p + \mathcal{K}} \hat{w}_s(a, \omega) + \frac{k_p}{k_p + \mathcal{K}} Q_1, \\ \hat{R}_2(\omega) = \frac{k_p \mathcal{K}}{k_p + \mathcal{K}} \hat{w}_s(-a, \omega) + \frac{k_p}{k_p + \mathcal{K}} Q_2. \end{cases} \quad (7)$$

Then, by substituting Eq. (7) into Eq. (6), the reaction forces applied on the beam can be found as follows:

$$\begin{cases} \hat{R}_1(\omega) = \Psi_1(\omega)Q_1 + \Gamma_1(\omega)Q_2, \\ \hat{R}_2(\omega) = \Psi_2(\omega)Q_1 + \Gamma_2(\omega)Q_2, \end{cases} \quad (8)$$

where the four functions are defined as follows:

$$\begin{cases} \Psi_1 = \frac{B_s [G(-a, \omega; -a) + \gamma(\omega)]}{\Phi(\omega)} - \mathcal{H}(\omega), & \Gamma_1 = \frac{-B_s G(a, \omega; a)}{\Phi(\omega)} - \mathcal{H}(\omega), \\ \Psi_2 = \frac{B_s [G(a, \omega; a) + \gamma(\omega)]}{\Phi(\gamma)} - \mathcal{H}(\omega), & \Gamma_2 = \frac{-B_s G(-a, \omega; -a)}{\Phi(\omega)} - \mathcal{H}(\omega), \end{cases}$$

where

$$\begin{cases} \Phi(\omega) = \mathcal{K} ([\gamma(\omega) + G(a, \omega; a)] [\gamma(\omega) + G(-a, \omega; -a)]), \\ \gamma(\omega) = B_s \frac{k_p + \mathcal{K}}{k_p \mathcal{K}}, \\ \mathcal{H}(\omega) = G(a, \omega; a)G(-a, \omega; a). \end{cases}$$

Eq. (8) provides analytical expressions for the reaction forces exerted on the beam. It should be remarked that in the symmetrical configuration, the problem can be simplified with the help of the following results:

$$\begin{cases} \Psi_1(\omega) = \Psi_2(\omega), \\ \Gamma_1(\omega) = \Gamma_2(\omega). \end{cases}$$

Eq. (8) shows the proportional relation of the reaction force in the function of two loads. By substituting this equation into Eq. (5), the total displacements of the cracked railway sleeper under moving loads can be computed. Notably, the reaction force is analytically calculated and is contingent on the track parameters. Furthermore, the reaction force exhibits a linear relationship with the moving loads.

3. NUMERIC EXAMPLE

The numerical examples of the presented model will be calculated using the parameters in Table 1. The parameters of the rail and the sleeper correspond to the rail UIC 60 and sleeper M450 which SATEBA produces, respectively. The other parameters are usual values found in published works by Hoang et al. [44], Tran et al. [20], Azoh et al. [45]. While the moving loads applied to the two rails are theoretically equal due to the symmetry of the problem, the distribution of loads from a single axle to the two rails is not equal as the train moves. Consequently, in this paper, the sleeper responses are calculated considering a non-symmetric load distribution: $P_1 = 0.9Q_1$ and $Q_1 = 100$ kN. The train speed is $v = 150$ km/h which corresponds to the operating speeds of typical French intercity trains such as Corail.

3.1. Validation of the model

To validate the proposed dynamic model, the results for an undamaged sleeper were compared with existing analytical models, particularly the model developed by Tran et al. [20]. Noting that this work developed the analytical model with a pre-stressed sleeper, so the effect of pre-stressed in the sleeper will not be considered in the comparison. The track parameters are shown in Table 1. The depth of the crack is: $k_\alpha = 0$. A finite element method (FEM) model was also developed using Cast3M software to provide numerical results for comparison [46].

Table 1. Parameters of the railway track

Content	Unit	Notation	Value
Flexural rigidity of rail	MNm ²	B_r	6.3
Linear mass density of rail	kgm ⁻¹	M_r	59.98
Stiffness of rail pad	MNm ⁻¹	k_{rp}	192
Damping coefficient of rail pad	MNsm ⁻¹	ζ_{rp}	1.97
Inter-sleeper distance	m	l	0.6
Flexural rigidity of sleeper	MNm ²	B_s	8.13
Linear mass density of sleeper	kgm ⁻¹	M_s	145.92
Sleeper length	m	$2L$	2.41
Linear stiffness coefficient of foundation	MNm ⁻²	k_f	182.57
Linear damping coefficient of foundation	MNsm ⁻²	ζ_f	24.4
Track gauge	m	$2a$	1.435

Figs. 4 and 5 present the comparison of the sleeper's displacement when the axle crosses it at a reference time $t = 0$. The red and yellow lines indicate the deformation calculated by the proposed model and by Tran et al. [20], respectively. The blue crosses represent the FEM results, while the black line shows the initial shape of the sleeper. The two dashed lines depict the positions of the two rails: rail 1 and rail 2 are colored green and purple, respectively.

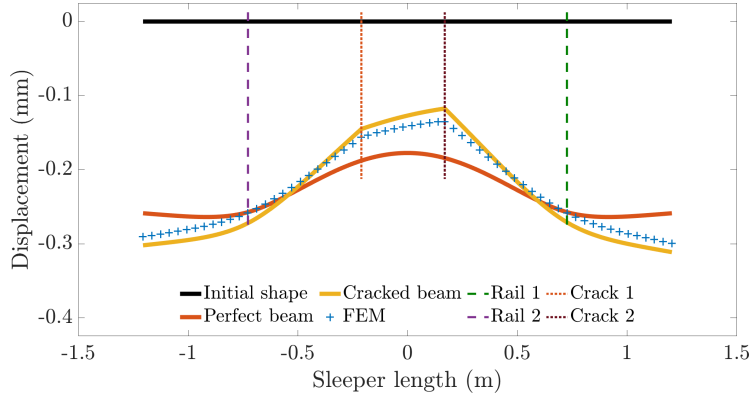


Fig. 4. Comparison of the rail deflections calculated by the models in the time domain, at the reference time $t = 0$: black continuous line: initial shape, golden continuous line: cracked beam, red continuous line: perfect beam, blue crosses: FEM model

The asymmetrical movement loads result in a non-symmetrical distortion of the sleeper. Notably, the proposed and current models exhibit good agreement, with a maximum discrepancy of less than 5% between the analytical and FEM models. In Fig. 4, the dotted purple line marks the position with maximum discrepancy of 4% of the FEM

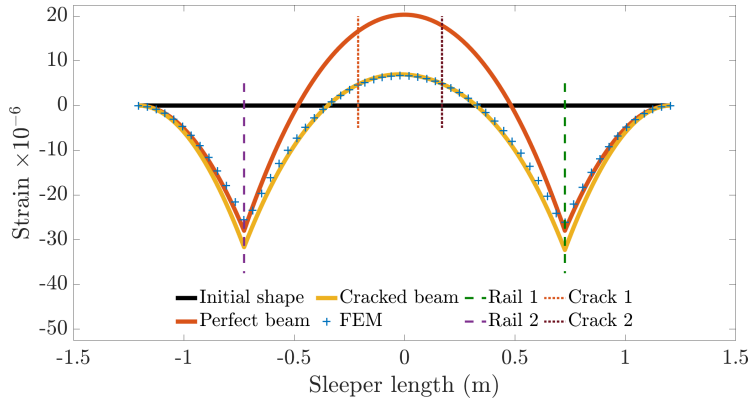


Fig. 5. Comparison of the rail strains calculated by the models in the time domain, at the reference time $t = 0$: black continuous line: initial shape, golden continuous line: cracked beam, red continuous line: perfect beam, blue crosses: FEM model

model (blue line) and analytical model (yellow line), in which two displacement values are written as 0.125 mm and 0.130 mm, respectively. This confirms the accuracy of both the proposed model and the FEM approach in predicting the sleeper's dynamic behavior under moving loads.

It should be noted that when $h_c = 0$, no discontinuity occurs. Hence, from a physical point of view: $\Delta\theta = 0$. On the other hand, mathematically, this phenomenon results in the following outcome: $k_c \rightarrow \infty$ (see Eq. (6)). Consequently, $C_h = 0$. Clearly, this specific scenario is adequately addressed by the model featuring a rotational spring, indicating that the beam remains undamaged when $h_c = 0$.

3.2. Case study: sleeper with 2 cracks

The occurrence of multiple cracks on sleeper structures is a common phenomenon and can be attributed to several factors. Firstly, uneven stress distribution on the surface of the sleeper can lead to the appearance of multiple cracks. Different areas of the surface may experience varying stress levels, resulting in the formation of multiple cracks. Secondly, cracks can interact with each other. When one crack forms, it can alter the surrounding structure and facilitate the formation of additional cracks, leading to a network of cracks. Thirdly, environmental and weather factors can cause the expansion and appearance of more cracks. This often occurs in outdoor structures, like railway sleepers, that are exposed to changing weather and environmental conditions. Lastly, the material characteristics play a crucial role. Different materials have varying capacities to withstand stress and environmental impacts. A lack of understanding in material design and usage can result in multiple cracks due to shortcomings in the design and construction process.

3.2.1. Two symmetrical cracks across the center of the sleeper

In reality, it is almost impossible for two cracks to be perfectly symmetrical across the center of the sleeper. However, to thoroughly understand the issue being investigated, this section will present a few special cases. These examples will illustrate the impact of crack characteristics (such as position and depth) on displacement and reaction forces at various points on the sleeper.

In the case of two cracks at the positions $x_{c1} = -0.25$ m, $x_{c2} = 0.25$ m and $x_{c1} = -1/3$ m, $x_{c2} = 1/3$ m, the sleeper nearly splits into two separate sections when one of the two cracks has a high ratio \bar{h} and the other crack has a low ratio \bar{h} . Additionally, the sleeper practically splits into three separate sections when both cracks have high ratios \bar{h}

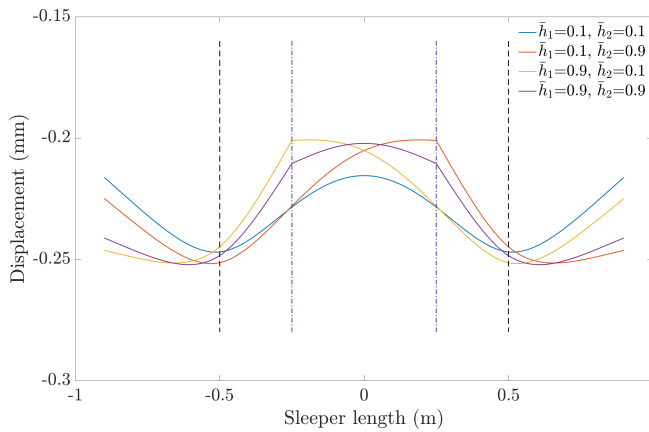


Fig. 6. Influence of crack depth on sleeper displacement at various positions and depths: $x_{c1} = -1/4$ m, $x_{c2} = 1/4$ m

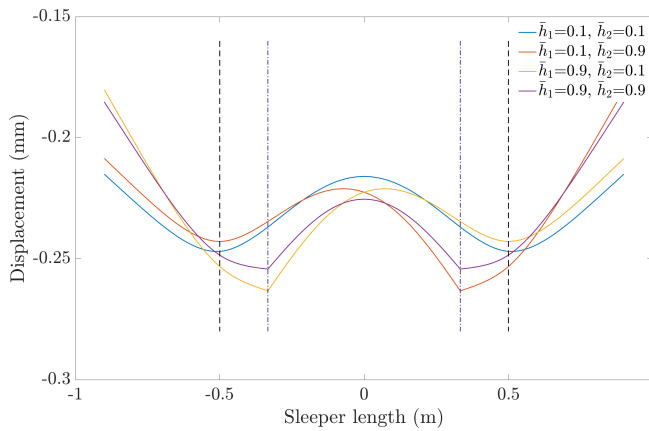


Fig. 7. Influence of crack depth on sleeper displacement at various positions and depths: $x_{c1} = -1/3$ m, $x_{c2} = 1/3$ m

(Figs. 6 and 7). However, when two cracks occur at the same location $x_{c_1} = -0.295$ m, $x_{c_2} = 0.295$ m, the displacement of the sleeper is hardly affected by the depth of the crack (Fig. 8).

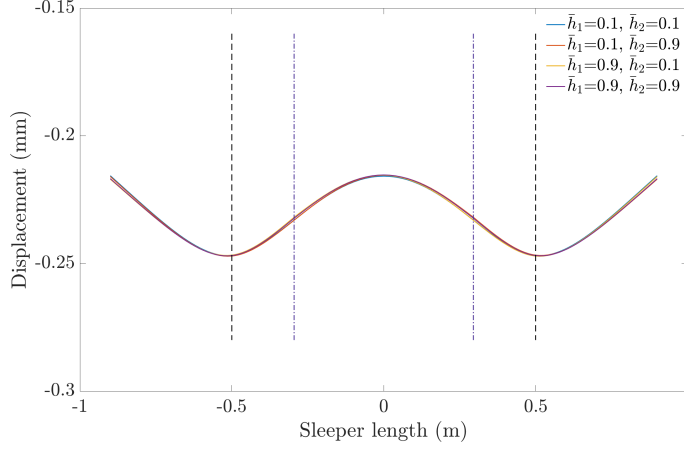


Fig. 8. Influence of crack depth on sleeper displacement at various positions and depths:
 $x_{c_1} = -0.295$ m, $x_{c_2} = 0.295$ m

The dynamic response of the track in the time domain is obtained numerically through the inverse Fourier transform. Assuming the wheel passes over the support at the reference time $t = 0$, Figs. 6–8 depict the deformed shape of the sleeper at this instant.

In the case of two cracks at the positions $x_{c_1} = -0.25$ m, $x_{c_2} = 0.25$ m, when increasing the depth of crack 1 and decreasing the depth of crack 2, the reaction force at the left rail increases (when \bar{h}_{c_1} reduces to zero, the problem returns to a single crack scenario). Conversely, when decreasing the depth of crack 1 and increasing the depth of crack 2, the reaction force at the left rail gradually decreases.

In the case of two cracks at the positions $x_{c_1} = -1/3$ m, $x_{c_2} = 1/3$ m, when increasing the depth of crack 1 and decreasing the depth of crack 2, the reaction force at the left rail increases (when \bar{h}_{c_2} reduces to zero, the problem returns to a single crack scenario). Conversely, when decreasing the depth of crack 1 and increasing the depth of crack 2, the reaction force at the left rail gradually decreases.

Due to the symmetric nature of this problem, a similar phenomenon will occur at the right rail. (Figs. 9–12).

In the case of two cracks at the positions $x_{c_1} = -0.295$ m, $x_{c_2} = 0.295$ m, similarly to the displacement, the discrepancy in reaction forces is also very small. At this position, the depth of the two cracks has little influence on the reaction forces at the two rails of the sleeper (as it is not located at the wave trough or wave node). However, in the long run, damage at this location also affects itself and adjacent sleepers, reducing their lifespan.

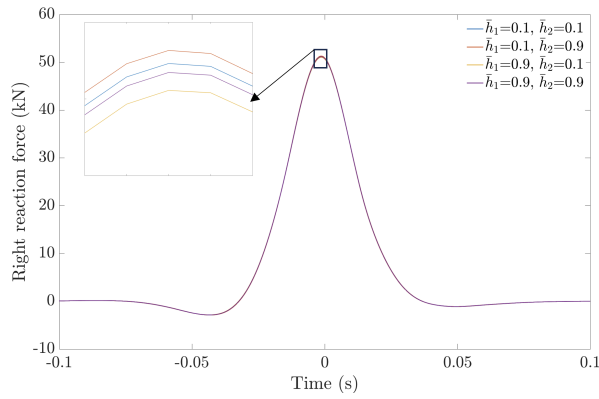


Fig. 9. The influence of the depth of the two cracks on the reaction force at the right rails:
(a), (b) $x_{c_1} = -1/4$ m, $x_{c_2} = 1/4$ m

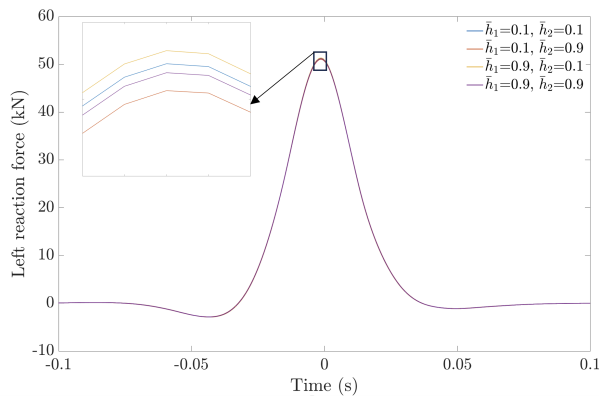


Fig. 10. The influence of the depth of the two cracks on the reaction force at the left rails:
(a), (b) $x_{c_1} = -1/4$ m, $x_{c_2} = 1/4$ m, (c), (d) $x_{c_1} = -1/3$ m, $x_{c_2} = 1/3$ m

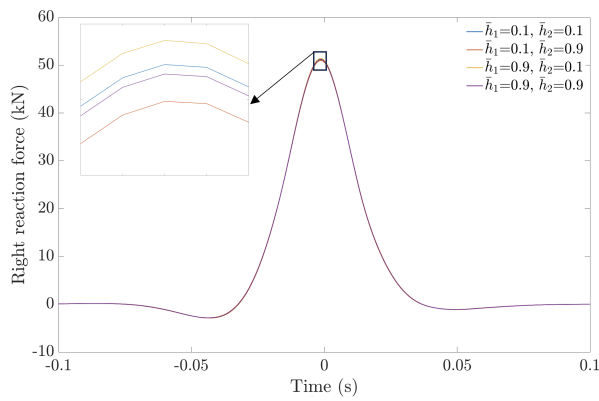


Fig. 11. The influence of the depth of the two cracks on the reaction force at the right rails:
 $x_{c_1} = -1/3$ m, $x_{c_2} = 1/3$ m

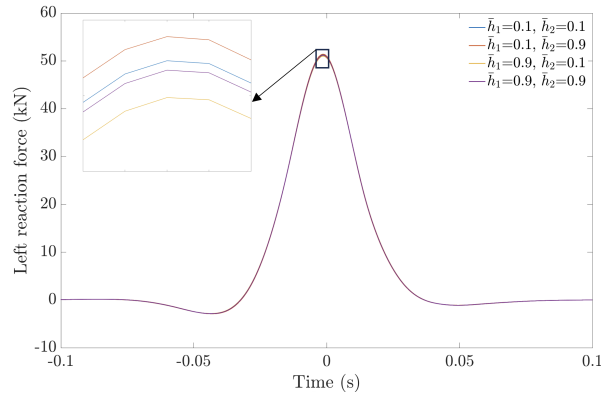


Fig. 12. The influence of the depth of the two cracks on the reaction force at the left rails:
 $x_{c_1} = -1/3 \text{ m}$, $x_{c_2} = 1/3 \text{ m}$

3.2.2. Two cracks in reality

Fig. 13 illustrates a scenario where two cracks appear on the sleeper in reality. In this research section, we examine the real-life case of crack occurrences as depicted in the figure, with two cracks located at two positions ($x_{c_1} = -0.21 \text{ m}$) and ($x_{c_2} = 0.17 \text{ m}$). The position $x = 0$ is considered as the center of the sleeper. The loads applied on the support are $Q_1 = Q_2 = 100 \text{ kN}$ at the positions of the two rails.

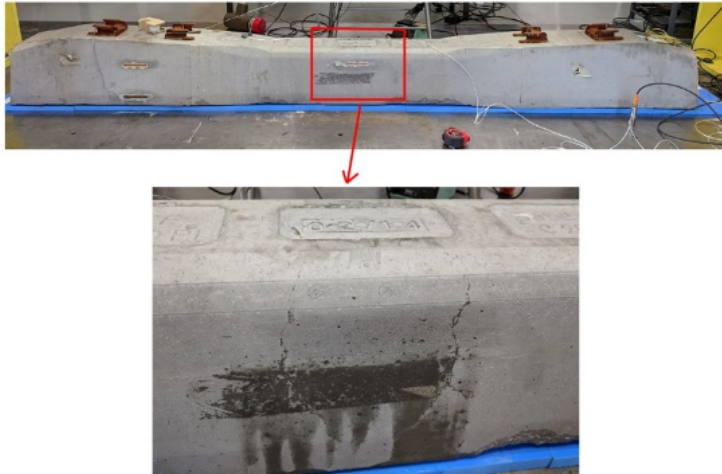


Fig. 13. The sleeper cracked (above) and close-up of the two cracks (below).

Figs. 14–16 illustrate the influence of the depth of the two cracks on the displacement of the sleeper in various scenarios. The sleeper practically splits into 2 or 3 separate sections as we alter the depth of the two cracks.

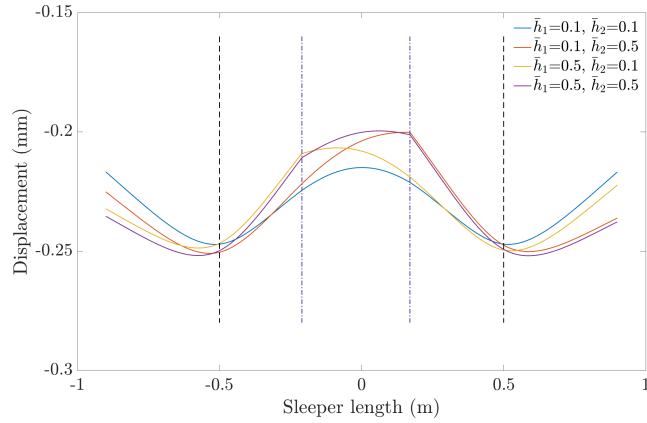


Fig. 14. The effect of the depth of the two cracks on the displacement of the sleeper with symmetrical loads and dis-symmetrical of crack positions: $x_{c1} = -0.21$ m and $x_{c2} = 0.17$ m

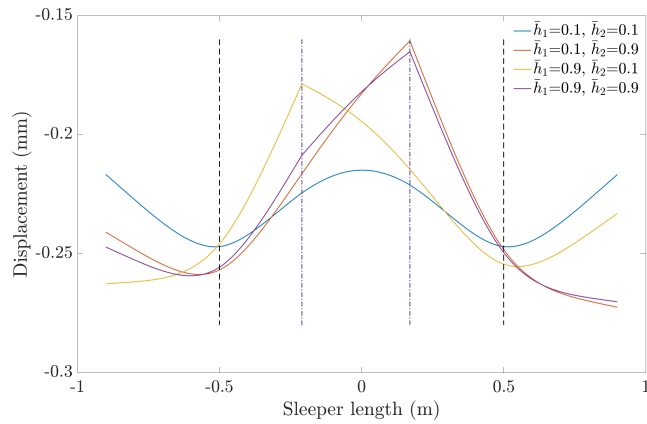


Fig. 15. The effect of the depth of the two cracks on the displacement of the sleeper with symmetrical loads and dis-symmetrical of crack positions: $x_{c1} = -0.21$ m and $x_{c2} = 0.17$ m

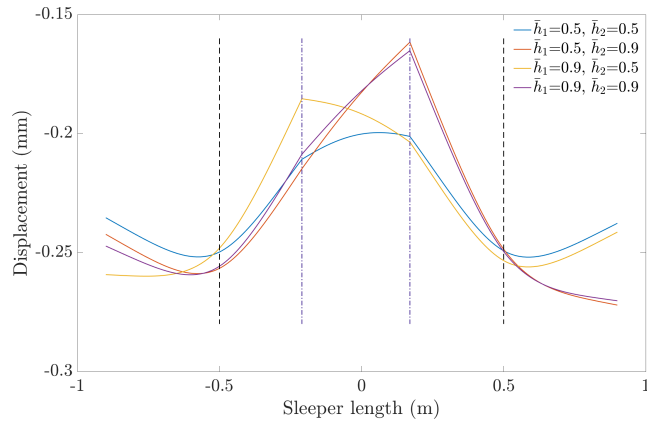


Fig. 16. The effect of the depth of the two cracks on the displacement of the sleeper with symmetrical loads and dis-symmetrical of crack positions: $x_{c1} = -0.21$ m and $x_{c2} = 0.17$ m

Table 2 and Fig. 17 show the displacement value of the sleeper at the left rail position based on the ratio \bar{h}_1 and \bar{h}_2 . When increasing the depth of crack 1 and decreasing the depth of crack 2, the displacement value at the left rail position decreases (when reducing the depth of crack 2 to 0, the problem reverts to a single crack scenario). Conversely, when decreasing the depth of crack 1 and increasing the depth of crack 2, the displacement at the left rail increases.

Table 2. The displacement value at the left rail depends on the depth of the crack (mm)

		\bar{h}_1								
		0.1	0.2	0.3	0.4	0.5	0.6	0.7	0.8	0.9
\bar{h}_2	0.1	0.2469	0.2474	0.2480	0.2490	0.2503	0.2518	0.2537	0.2553	0.2566
	0.2	0.2469	0.2473	0.2480	0.2489	0.2502	0.2517	0.2536	0.2553	0.2566
	0.3	0.2468	0.2471	0.2479	0.2488	0.2502	0.2515	0.2535	0.2552	0.2565
	0.4	0.2467	0.2471	0.2477	0.2486	0.2498	0.2513	0.2533	0.2550	0.2564
	0.5	0.2466	0.2470	0.2475	0.2484	0.2495	0.2510	0.2530	0.2548	0.2562
	0.6	0.2465	0.2469	0.2474	0.2481	0.2492	0.2507	0.2527	0.2546	0.2560
	0.7	0.2464	0.2467	0.2472	0.2480	0.2489	0.2504	0.2524	0.2542	0.2560
	0.8	0.2463	0.2466	0.2471	0.2479	0.2486	0.2502	0.2521	0.2537	0.2557
	0.9	0.2457	0.2459	0.2463	0.2470	0.2479	0.2491	0.2511	0.2533	0.2554

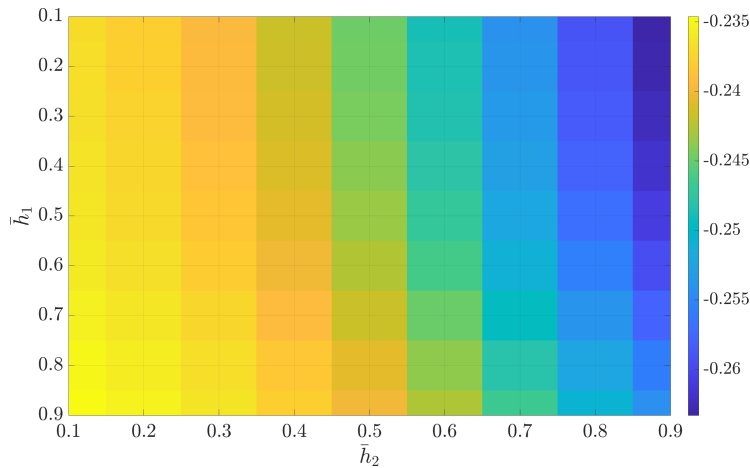


Fig. 17. The influence of the depth of the two cracks on the displacement at various positions - Displacement at the left rail (mm)

At the right rail, the displacement value decreases as the depth of both cracks decreases. Additionally, the displacement value increases when the depth of crack 1 increases and the depth of crack 2 decreases. This is clearly illustrated in the data Table 3 and Fig. 18.

Table 3. The displacement value at the right rail depends on the depth of the crack (mm)

		\bar{h}_1								
		0.1	0.2	0.3	0.4	0.5	0.6	0.7	0.8	0.9
\bar{h}_2	0.1	0.2469	0.2470	0.2470	0.2471	0.2473	0.2475	0.2477	0.2479	0.2480
	0.2	0.2472	0.2473	0.2473	0.2474	0.2475	0.2476	0.2478	0.2479	0.2480
	0.3	0.2477	0.2477	0.2478	0.2478	0.2478	0.2479	0.2480	0.2480	0.2481
	0.4	0.2484	0.2484	0.2484	0.2484	0.2483	0.2483	0.2482	0.2482	0.2482
	0.5	0.2494	0.2493	0.2493	0.2492	0.2490	0.2489	0.2486	0.2484	0.2483
	0.6	0.2505	0.2504	0.2503	0.2501	0.2499	0.2496	0.2492	0.2488	0.2484
	0.7	0.2519	0.2518	0.2517	0.2514	0.2511	0.2506	0.2499	0.2493	0.2487
	0.8	0.2532	0.2531	0.2529	0.2526	0.2522	0.2516	0.2507	0.2498	0.2490
	0.9	0.2542	0.2541	0.2539	0.2536	0.2531	0.2525	0.2515	0.2503	0.2492

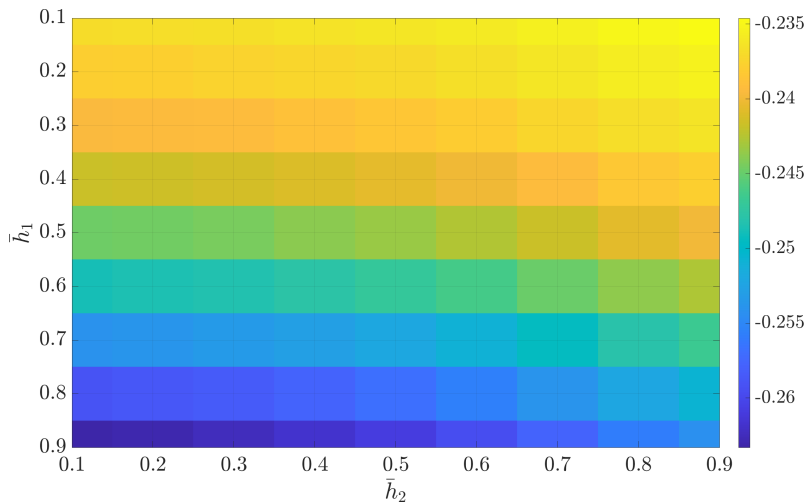


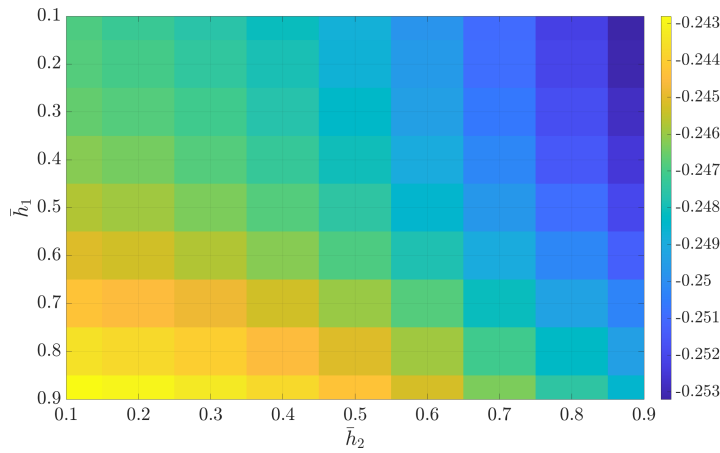
Fig. 18. The influence of the depth of the two cracks on the displacement at various positions - Displacement at the right rail (mm)

At the positions x_{c1} , the displacement value increases as the depth of both cracks decreases (when the depth of both cracks decreases to 0, the displacement at crack 1 reaches its maximum value). When increasing the depth of crack 1 and decreasing the depth of crack 2, the displacement value at position x_{c1} decreases (when reducing the depth of crack 2 to 0, the problem reverts to a single crack scenario). This is clearly illustrated in the data Table 4 and Fig. 19.

At the position (x_{c2}), similar to the position (x_{c1}), the displacement value increases as the depth of both cracks decreases (when the depth of both cracks decreases to 0, the displacement at crack 2 reaches its maximum value). When increasing the depth

Table 4. The displacement value at position x_{c_1} depends on the depth of the crack (mm)

		\bar{h}_1								
		0.1	0.2	0.3	0.4	0.5	0.6	0.7	0.8	0.9
\bar{h}_2	0.1	0.2245	0.2241	0.2235	0.2227	0.2216	0.2203	0.2187	0.2173	0.2163
	0.2	0.2225	0.2222	0.2218	0.2211	0.2203	0.2193	0.2180	0.2169	0.2161
	0.3	0.2193	0.2192	0.2189	0.2186	0.2181	0.2176	0.2169	0.2162	0.2158
	0.4	0.2149	0.2149	0.2149	0.2149	0.2150	0.2151	0.2151	0.2152	0.2153
	0.5	0.2090	0.2093	0.2096	0.2101	0.2108	0.2116	0.2127	0.2137	0.2146
	0.6	0.2018	0.2022	0.2029	0.2039	0.2052	0.2070	0.2094	0.2116	0.2136
	0.7	0.1929	0.1935	0.1945	0.1959	0.1979	0.2007	0.2046	0.2085	0.2120
	0.8	0.1849	0.1856	0.1868	0.1885	0.1910	0.1945	0.1997	0.2051	0.2103
	0.9	0.1786	0.1794	0.1806	0.1825	0.1852	0.1892	0.1952	0.2019	0.2085

Fig. 19. The influence of the depth of the two cracks on the displacement at various positions - Displacement at the crack x_{c_1} (mm)

of crack 2 and decreasing the depth of crack 1, the displacement value at position (x_{c_2}) decreases (when reducing the depth of crack 1 to 0, the problem reverts to a single crack scenario). This is clearly demonstrated in the data Table 5 and Fig. 20.

Table 5. The displacement value at position x_{c_2} depends on the depth of the crack (mm)

		\bar{h}_1								
		0.1	0.2	0.3	0.4	0.5	0.6	0.7	0.8	0.9
\bar{h}_2	0.1	0.2212	0.2184	0.2141	0.2080	0.2002	0.1906	0.1788	0.1685	0.1605
	0.2	0.2209	0.2182	0.2139	0.2080	0.2003	0.1908	0.1790	0.1687	0.1606

		\bar{h}_1								
		0.1	0.2	0.3	0.4	0.5	0.6	0.7	0.8	0.9
\bar{h}_2	0.3	0.2204	0.2178	0.2137	0.2080	0.2005	0.1911	0.1795	0.1690	0.1608
	0.4	0.2197	0.2173	0.2135	0.2080	0.2008	0.1916	0.1801	0.1695	0.1610
	0.5	0.2189	0.2167	0.2131	0.2080	0.2011	0.1923	0.1809	0.1702	0.1614
	0.6	0.2178	0.2159	0.2126	0.2080	0.2016	0.1933	0.1821	0.1712	0.1620
	0.7	0.2165	0.2148	0.2121	0.2080	0.2023	0.1946	0.1837	0.1727	0.1629
	0.8	0.2153	0.2139	0.2115	0.2080	0.2029	0.1958	0.1854	0.1743	0.1640
	0.9	0.2144	0.2132	0.2111	0.2080	0.2034	0.1969	0.1870	0.1759	0.1650

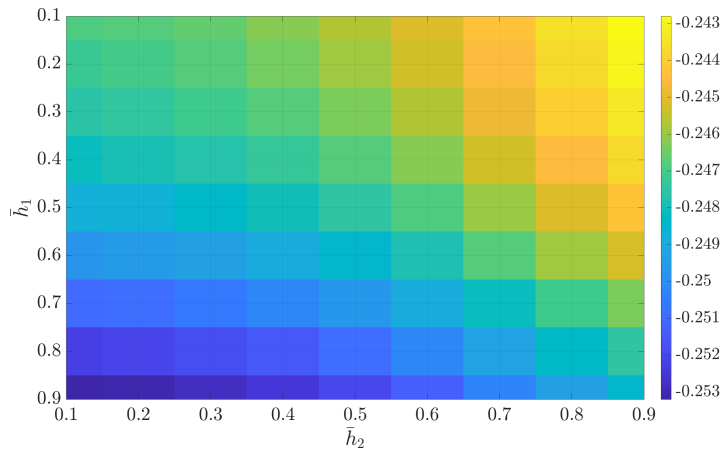


Fig. 20. The influence of the depth of the two cracks on the displacement at various positions - Displacement at the crack x_{c_2} (mm)

Table 6. The reaction force value at the right rail depends on the depth of the crack (kN)

		\bar{h}_1								
		0.1	0.2	0.3	0.4	0.5	0.6	0.7	0.8	0.9
\bar{h}_2	0.1	50.8472	50.8454	50.8426	50.8376	50.8336	50.8274	50.8198	50.8131	50.8079
	0.2	50.8355	50.8342	50.8322	50.8294	50.8257	50.8211	50.8155	50.8106	50.8067
	0.3	50.8167	50.8162	50.8154	50.8142	50.8127	50.8108	50.8085	50.8064	50.8047
	0.4	50.7905	50.7910	50.7917	50.7928	50.7941	50.7950	50.7981	50.8001	50.8017
	0.5	50.7563	50.7579	50.7604	50.7641	50.7690	50.7752	50.7834	50.7910	50.7972
	0.6	50.7139	50.7166	50.7210	50.7275	50.7363	50.7480	50.7633	50.7802	50.7908
	0.7	50.6619	50.6650	50.6712	50.6804	50.6923	50.7105	50.7347	50.7593	50.7810
	0.8	50.6144	50.6187	50.6260	50.6368	50.6523	50.6738	50.7035	50.7347	50.7699
	0.9	50.5775	50.5821	50.5898	50.6013	50.6423	50.6787	50.6787	50.7193	50.7588

At the right rail, the reaction force increases as the depth of both cracks decreases (when the depth of both cracks decreases to 0, the reaction force at the right rail reaches its maximum value). When increasing the depth of crack 1 and decreasing the depth of crack 2, the reaction force at the right rail decreases (when the depth of crack 2 decreases to 0, the problem reverts to a single crack scenario). This is clearly demonstrated in Table 6 and Fig. 21.

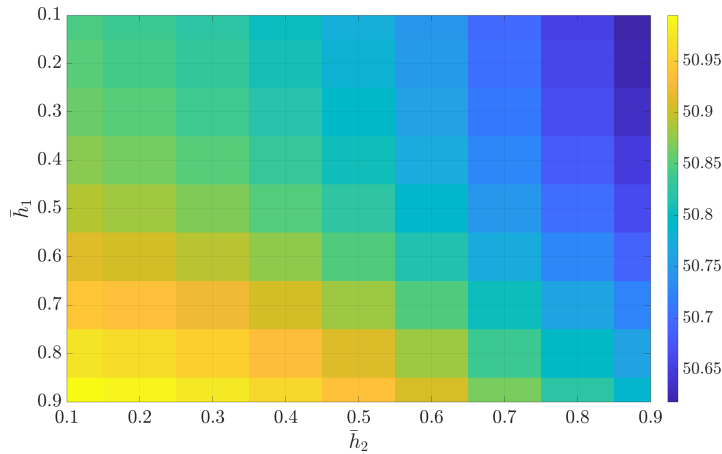


Fig. 21. The influence of the depth of the two cracks on the reaction force at the two rails - Reaction force at the left rail (kN)

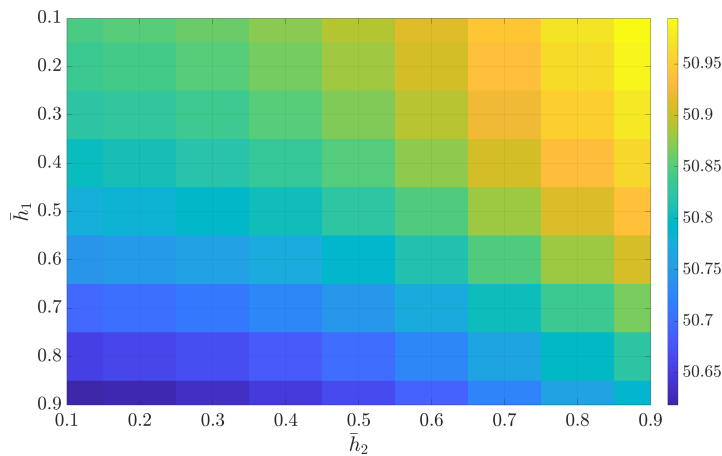


Fig. 22. The influence of the depth of the two cracks on the reaction force at the two rails - Reaction force at the right rail

At the left rail, increasing the depth of crack 1 and decreasing the depth of crack 2 results in an increase in the reaction force (when the depth of crack 2 decreases to 0, the

problem reverts to a single crack scenario). Conversely, decreasing the depth of crack 1 and increasing the depth of crack 2 leads to a decrease in the reaction force at the left rail. Detailed data is presented in Table 6 and Fig. 22.

4. CONCLUSIONS

This study presents an analytical model to evaluate the dynamic behavior of railway sleepers subjected to moving loads, with a focus on the influence of cracks. The Euler–Bernoulli beam theory was used, and cracks were modeled as rotational springs, with their stiffness based on crack depth. The dynamical responses were determined using Green’s function in the frequency domain, and a finite element model was developed to validate the analytical solutions. The results show that the presence of cracks significantly affects the dynamic behavior of the sleeper, reducing its stiffness and altering the reaction forces at the rails. The numerical parametric study demonstrates the effects of crack depth and position on the dynamic response of damaged sleepers. The results also highlight the importance of monitoring and maintaining sleepers to prevent structural failures due to crack propagation. Future research could explore the impact of imperfections in the rail-wheel contact and investigate alternative foundation models to further improve the accuracy of the dynamic analysis.

DECLARATION OF COMPETING INTEREST

The authors declare that they have no known competing financial interests or personal relationships that could have appeared to influence the work reported in this paper.

FUNDING

This research received no specific grant from any funding agency in the public, commercial, or not-for-profit sectors.

REFERENCES

- [1] E. Winkler. *Vorträge über Eisenbahnbau*, Vol. 11. H. Dominicus, (1878).
- [2] P. Pasternak. Basis of a new method for the calculation of structures on elastic foundation using two bed constants. *Gosstroizdat*, (1954). (in Russian).
- [3] V. Vlasov and N. Leontiev. Technical theory of analysis of foundations on an elastic base. *MISI Sbornik Trudov*, **14**, (1956).
- [4] A. D. Kerr. Elastic and viscoelastic foundation models. *Journal of Applied Mechanics*, **81**, (1964), pp. 491–498. <https://doi.org/10.1115/1.3629667>.
- [5] G. D. Zhang and B. Z. Guo. On the spectrum of Euler–Bernoulli beam equation with Kelvin–Voigt damping. *Journal of Mathematical Analysis and Applications*, **374**, (2011), pp. 210–229. <https://doi.org/10.1016/j.jmaa.2010.08.070>.

- [6] F. Hassine. Logarithmic stabilization of the Euler–Bernoulli transmission plate equation with locally distributed Kelvin–Voigt damping. *Journal of Mathematical Analysis and Applications*, **455**, (2017), pp. 1765–1782. <https://doi.org/10.1016/j.jmaa.2017.06.068>.
- [7] M. Javadi and M. Rahmanian. Nonlinear vibration of fractional Kelvin–Voigt viscoelastic beam on nonlinear elastic foundation. *Communications in Nonlinear Science and Numerical Simulation*, **98**, (2021). <https://doi.org/10.1016/j.cnsns.2021.105784>.
- [8] Y. Lei, S. Adhikari, and M. I. Friswell. Vibration of nonlocal Kelvin–Voigt viscoelastic damped Timoshenko beams. *International Journal of Engineering Science*, **66–67**, (2013), pp. 1–13. <https://doi.org/10.1016/j.ijengsci.2013.02.004>.
- [9] W. R. Chen. Bending vibration of axially loaded Timoshenko beams with locally distributed Kelvin–Voigt damping. *Journal of Sound and Vibration*, **330**, (2011), pp. 3040–3056. <https://doi.org/10.1016/j.jsv.2011.01.015>.
- [10] W. R. Chen. Vibration analysis of twisted Timoshenko beams with internal Kelvin–Voigt damping. *Procedia Engineering*, **67**, (2013), pp. 525–532. <https://doi.org/10.1016/j.proeng.2013.12.053>.
- [11] W. R. Chen. Effect of local Kelvin–Voigt damping on eigenfrequencies of cantilevered twisted Timoshenko beams. *Procedia Engineering*, **79**, (2014), pp. 160–165. <https://doi.org/10.1016/j.proeng.2014.06.325>.
- [12] W. R. Chen. Parametric studies on bending vibration of axially-loaded twisted Timoshenko beams with locally distributed Kelvin–Voigt damping. *International Journal of Mechanical Sciences*, **88**, (2014), pp. 61–70. <https://doi.org/10.1016/j.ijmecsci.2014.07.006>.
- [13] P. S. P. Zhang and H. Qing. Stress-driven local/nonlocal mixture model for buckling and free vibration of FG sandwich Timoshenko beams resting on a nonlocal elastic foundation. *Composite Structures*, **289**, (2022). <https://doi.org/10.1016/j.compstruct.2022.115473>.
- [14] P. S. P. Zhang and H. Qing. Unified two-phase nonlocal formulation for vibration of functionally graded beams resting on nonlocal viscoelastic Winkler–Pasternak foundation. *Applied Mathematics and Mechanics*, **44**, (2023), pp. 89–108. <https://doi.org/10.1007/s10483-023-2948-9>.
- [15] L. Fryba. *Vibration of solids and structures under moving loads*. Springer Netherlands, (1972). <https://doi.org/10.1007/978-94-011-9685-7>.
- [16] V. H. Nguyen and D. Duhamel. Finite element procedures for nonlinear structures in moving coordinates. part 1: Infinite bar under moving axial loads. *Computers and Structures*, **84**, (2006), pp. 1368–1380. <https://doi.org/10.1016/j.compstruc.2006.02.018>.
- [17] V. H. Nguyen and D. Duhamel. Finite element procedures for nonlinear structures in moving coordinates. Part II: Infinite beam under moving harmonic loads. *Computers and Structures*, **86**, (2008), pp. 2056–2063. <https://doi.org/10.1016/j.compstruc.2008.04.010>.
- [18] P. C. Jorge, F. Simoes, and A. P. da Costa. Dynamics of beams on non-uniform nonlinear foundations subjected to moving loads. *Computers and Structures*, **148**, (2014), pp. 26–34. <https://doi.org/10.1016/j.compstruc.2014.11.002>.
- [19] L. H. Tran, T. Hoang, D. Duhamel, G. Foret, S. Messad, and A. Loac. Analytical model of the dynamics of railway sleeper. In *Proceedings of the 6th International Conference on Computational Methods in Structural Dynamics and Earthquake Engineering (COMPADYN 2015)*, Institute of Structural Analysis and Antiseismic Research School of Civil Engineering National Technical University of Athens (NTUA) Greece, COMPADYN 2017, (2017), pp. 3937–3948. <https://doi.org/10.7712/120117.5695.18372>.

- [20] L. H. Tran, T. Hoang, G. Foret, D. Duhamel, S. Messad, and A. Loaec. A fast analytic method to calculate the dynamic response of railways sleepers. *Journal of Vibration and Acoustics*, **141**, (2018), pp. 1368–1380. <https://doi.org/10.1115/1.4040392>.
- [21] L. H. Tran, T. Hoang, G. Foret, D. Duhamel, S. Messad, and A. Loaec. Influence of non-homogeneous foundations on the dynamic responses of railway sleepers. *International Journal of Structural Stability and Dynamics*, **21**, (2021). <https://doi.org/10.1142/s0219455421500024>.
- [22] L. H. Tran, K. Le-Nguyen, and T. Hoang. A comparison of beam models for the dynamics of railway sleepers. *International Journal of Rail Transportation*, **11**, (2022), pp. 92–110. <https://doi.org/10.1080/23248378.2022.2034062>.
- [23] L.-H. Tran and K. Le-Nguyen. Calculation of dynamic responses of a cracked beam on visco-elastic foundation subjected to moving loads, and its application to a railway track model. *International Journal of Applied Mechanics*, **15**, (2023). <https://doi.org/10.1142/s1758825123500266>.
- [24] L.-H. Tran, T.-M. Duong, T. Hoang, G. Foret, and D. Duhamel. An analytical model to calculate the forced vertical vibrations of two rails subjected to the dynamic loads of ballasted railway track. *Structures*, **68**, (2024). <https://doi.org/10.1016/j.istruc.2024.107203>.
- [25] L.-H. Tran, T.-M. Duong, B. Claudet, K. Le-Nguyen, A. Nordborg, and F. Schmidt. Comparative analysis of beam models for vertical rail vibrations under dynamic forces. *European Journal of Mechanics - A/Solids*, **110**, (2025). <https://doi.org/10.1016/j.euromechsol.2024.105497>.
- [26] P. Fieguth and S. Sinha. Automated analysis and detection of cracks in underground scanned pipes. In *Proceedings 1999 International Conference on Image Processing (Cat. 99CH36348)*, IEEE, Vol. 4 of ICIP-99, (1999), pp. 395–399. <https://doi.org/10.1109/icip.1999.819622>.
- [27] Q. Feng, Q. Kong, L. Huo, and G. Song. Crack detection and leakage monitoring on reinforced concrete pipe. *Smart Materials and Structures*, **24**, (2015). <https://doi.org/10.1088/0964-1726/24/11/115020>.
- [28] R. D. Adams, P. Cawley, C. J. Pye, and B. J. Stone. A vibration technique for non-destructively assessing the integrity of structures. *Journal of Mechanical Engineering Science*, **20**, (2), (1978), pp. 93–100. <https://doi.org/10.1243/jmes.jour.1978.020.016.02>.
- [29] H. J. Petroski. Simple static and dynamic models for the cracked elastic beam. *International Journal of Fracture*, **17**, (1981), pp. R71–R76. <https://doi.org/10.1007/bf00036201>.
- [30] J. Lemaitre. *Handbook of materials behavior models*, Vol. 1-3. Academic Press, (2001).
- [31] N. T. Khiem and T. V. Lien. A simplified method for natural frequency analysis of a multiple cracked beam. *Journal of Sound and Vibration*, **245**, (2001), pp. 737–751. <https://doi.org/10.1006/jsvi.2001.3585>.
- [32] S. P. Lele and S. K. Maiti. Modelling of transverse vibration of short beams for crack detection and measurement of crack extension. *Journal of Sound and Vibration*, **257**, (2002), pp. 559–583. <https://doi.org/10.1006/jsvi.2002.5059>.
- [33] E. Viola, L. Federici, and L. Nobile. Detection of crack location using cracked beam element method for structural analysis. *Theoretical and Applied Fracture Mechanics*, **36**, (2001), pp. 23–35. [https://doi.org/10.1016/s0167-8442\(01\)00053-2](https://doi.org/10.1016/s0167-8442(01)00053-2).
- [34] S. H. S. Carneiro and D. J. Inman. Continuous model for the transverse vibration of cracked Timoshenko beams. *Journal of Vibration and Acoustics*, **124**, (2), (2002), pp. 310–320. <https://doi.org/10.1115/1.1452744>.

- [35] J. L. Hearndon, G. P. Potirniche, D. Parker, P. M. Cuevas, H. Rinehart, P. T. Wang, and M. F. Horstemeyer. Monitoring structural damage of components using an effective modulus approach. *Theoretical and Applied Fracture Mechanics*, **50**, (2008), pp. 23–29. <https://doi.org/10.1016/j.tafmec.2008.04.002>.
- [36] A. C. Batihan and F. S. Kadioglu. Vibration analysis of a racked beam on an elastic foundation. *International Journal of Structural Stability and Dynamics*, **16**, (05), (2016). <https://doi.org/10.1142/s0219455415500066>.
- [37] H. Darban, R. Luciano, and M. Basista. Free transverse vibrations of nanobeams with multiple cracks. *International Journal of Engineering Science*, **177**, (2022). <https://doi.org/10.1016/j.ijengsci.2022.103703>.
- [38] J. A. Loya, L. Rubio, and J. Fernández-Sáez. Natural frequencies for bending vibrations of Timoshenko cracked beams. *Journal of Sound and Vibration*, **290**, (2006), pp. 640–653. <https://doi.org/10.1016/j.jsv.2005.04.005>.
- [39] J. A. Loya, J. Aranda-Ruiz, and R. Zaera. Natural frequencies of vibration in cracked Timoshenko beams within an elastic medium. *Theoretical and Applied Fracture Mechanics*, **118**, (2022). <https://doi.org/10.1016/j.tafmec.2022.103257>.
- [40] T.-S. Pham, T. Hoang, D. Duhamel, G. Forêt, F. Schmidt, F.-B. Cartiaux, and V. Le Corvec. Dynamic response of a cracked multi-span continuous beam subjected to a moving multi-axle vehicle load. In *International Conference on Structural Health Monitoring of Intelligent Infrastructure*, (2021).
- [41] T. Yan, S. Kitipornchai, J. Yang, and X. Q. He. Dynamic behaviour of edge-cracked shear deformable functionally graded beams on an elastic foundation under a moving load. *Composite Structures*, **93**, (2011), pp. 2992–3001. <https://doi.org/10.1016/j.compstruct.2011.05.003>.
- [42] M. Rezaiee-Pajand and N. Gharaei-Moghaddam. A force-based rectangular cracked element. *International Journal of Applied Mechanics*, **13**, (2021). <https://doi.org/10.1142/s1758825121500472>.
- [43] S. Zheng, R. Huang, R. Lin, and Z. Liu. A phase field solution for modelling hyperelastic material and hydrogel fracture in ABAQUS. *Engineering Fracture Mechanics*, **276**, (2022). <https://doi.org/10.1016/j.engfracmech.2022.108894>.
- [44] T. Hoang, D. Duhamel, G. Foret, H. Yin, P. Joyez, and R. Caby. Calculation of force distribution for a periodically supported beam subjected to moving loads. *Journal of Sound and Vibration*, **388**, (2017), pp. 327–338. <https://doi.org/10.1016/j.jsv.2016.10.031>.
- [45] T. S. Azoh, W. Nzie, B. Djeumako, and B. S. Fotsing. Modeling of train track vibrations for maintenance perspectives: Application. *European Scientific Journal*, **10**, (21), (2014), pp. 260–275.
- [46] E. L. Fichoux. *Presentation et utilisation de Cast3M*. Support of CEA, (2011).
- [47] J. Fernandez-Saez, L. Rubio, and C. Navarro. Approximate calculation of the fundamental frequency for bending vibrations of cracked beams. *Journal of Sound and Vibration*, **225**, (1999), pp. 345–352. <https://doi.org/10.1006/jsvi.1999.2251>.
- [48] T. G. Chondros and A. D. Dimarogonas. Vibration of a cracked cantilever beam. *Journal of Vibration and Acoustics*, **120**, (1998), pp. 742–746. <https://doi.org/10.1115/1.2893892>.
- [49] X. Zhao, Y. R. Zhao, X. Z. Gao, X. Y. Li, and Y. H. Li. Greens functions for the forced vibrations of cracked Euler-Bernoulli beams. *Mechanical Systems and Signal Processing*, **68–69**, (2016), pp. 155–175. <https://doi.org/10.1016/j.ymsp.2015.06.023>.

APPENDIX A. CRACKED BEAM ON A VISCO-ELASTIC FOUNDATION SUBJECTED TO MOVING LOADS

The focus is on a dynamic model of the cracked beam posed on a visco-elastic foundation, as illustrated in Fig. A.1. Within this framework, the dynamic behaviors of the beam are described using the Euler–Bernoulli beam model. The beam has length L ($0 \leq x \leq L$) and is posed on the Kelvin–Voigt foundation which is characterized by stiffness k_f and damping coefficient ζ_f . In the time domain, the dynamic vertical displacement $w_i(x, t)$ of the beam can be defined by Eq. (1) in Section 2. The moving load applied at the coordinate $x = a$ can be written as follows:

$$F(x, t) = -R(t)\delta(x - a). \quad (\text{A.1})$$

Through the utilization of Fourier’s transform and the inclusion of Eq. (A.1), Eq. (1) can be expressed in the frequency domain as follows:

$$\frac{\partial^4 \hat{w}_s(x, \omega)}{\partial x^4} - \frac{\omega^2 M_s - k_s}{B_s} \hat{w}_s(x, \omega) = -\frac{\hat{R}(\omega)}{B_s} \delta(x - a), \quad (\text{A.2})$$

where $\hat{w}_s(x, \omega)$ is the displacement of the beam in the frequency domain and the stiffness dynamic of the foundation k_b is defined as $k_b = k_f + j\omega\zeta_f$.

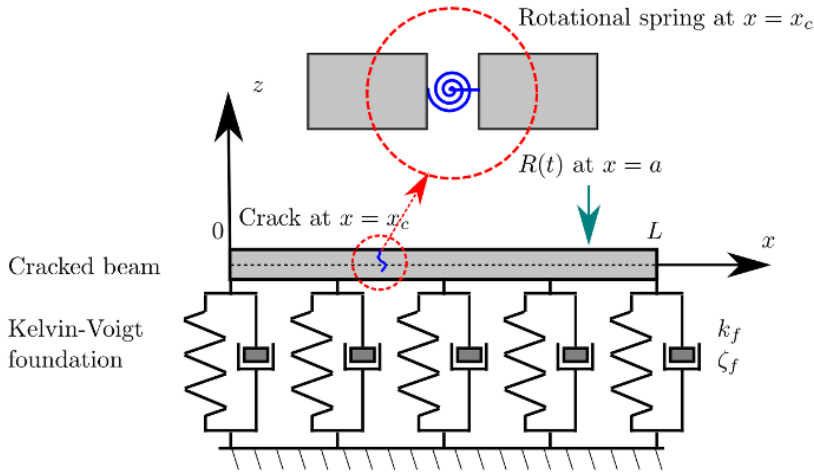


Fig. A.1. Modeling a cracked beam situated on a Kelvin–Voigt foundation under the influence of moving loads

Eq. (A.2) describes the beam responses. To solve this equation, we will employ Green’s function, determined as follows:

$$\frac{\partial^4 G(x, \omega, a)}{\partial x^4} - \lambda_s^4 G(x, \omega, a) = \delta(x - a), \quad (\text{A.3})$$

where $\lambda_s = \sqrt[4]{\frac{\omega^2 M_s - k_s}{B_s}}$. Given that the amplitude of the reaction force depends solely on the angular velocity, Eq. (A.3) represents a partially normalized form of Eq. (A.2). The general solution of this fourth-order linear differential equation is provided by:

$$G(x, \omega, a) = \begin{cases} A_1 \cos \lambda_s x + A_2 \sin \lambda_s x + A_3 \cosh \lambda_s x + A_4 \sinh \lambda_s x, & \forall x \in [0, a] \\ B_1 \cos \lambda_s x + B_2 \sin \lambda_s x + B_3 \cosh \lambda_s x + B_4 \sinh \lambda_s x, & \forall x \in [a, L] \end{cases} \quad (\text{A.4})$$

In Eq. (A.4), the 8 constants $A_{1,2,3,4}$ and $B_{1,2,3,4}$ are determined to meet the following conditions:

- Condition of a free-free beam at both ends of the beam can be written as follows:

$$\begin{cases} \frac{\partial^2 G(0, \omega, a)}{\partial x^2} = \frac{\partial^2 G(L, \omega, a)}{\partial x^2} = 0, \\ \frac{\partial^3 G(0, \omega, a)}{\partial x^3} = \frac{\partial^3 G(L, \omega, a)}{\partial x^3} = 0. \end{cases}$$

- Continuity of displacement, slope and moment at $x = a$ can be displayed as follows:

$$\begin{cases} G(a^+, \omega, a) - G(a^-, \omega, a) = 0, \\ \frac{\partial G(a^+, \omega, a)}{\partial x} - \frac{\partial G(a^-, \omega, a)}{\partial x} = 0, \\ \frac{\partial^2 G(a^+, \omega, a)}{\partial x^2} - \frac{\partial^2 G(a^-, \omega, a)}{\partial x^2} = 0. \end{cases}$$

- Shear force discontinuity of magnitude one at $x = a$ can be shown as follows:

$$\frac{\partial^3 G(a^+, \omega, a)}{\partial x^3} - \frac{\partial^3 G(a^-, \omega, a)}{\partial x^3} = \frac{1}{B_s}.$$

In this study, considering that n open cracks are on a single side of the beam, each with depth h_j ($j = [1, n]$), it can be learned that at the n positions x_e situated in the interval $x \in [0, a]$. As a result of these cracks, discontinuities are introduced into the beam.

Consequently, the beam is now segmented into $n + 1$ separate segments, each with a length L_j . The separated beams are linked by massless rotational springs with sectional flexibility. In this model, the effect of bending deflection is assumed to be negligible. The discontinuity in the slope of the beam deflection can be found as follows:

$$\Delta\theta = \frac{M}{k_e},$$

where M is the bending moment at the cracked cross-section and k_e is the stiffness of the rotational spring defined as follows:

$$k_e = \frac{B}{hC_i}$$

where h is the height of the beam and C_i is the non-dimensional constant evaluated by using different methods (starting from the strain energy density in fracture mechanics [47]) or developing the fracture mechanics model to evaluate using a lumped flexibility approach [48]. Usually, this constant can be found as a function of \bar{h} means the ratio between the depth of the crack and the height of the beam for different cross-sectional forms. For the rectangular cross section, [49] suggested a relationship between the non-dimensional constant for two cases of \bar{h} as follows:

- With $\bar{h} \in [0, 0.6]$:

$$C(\bar{h}) = 6\pi(1 - \nu^2)\bar{h}^2(0.6272 - 1.04533\bar{h} + 4.5948\bar{h}^2 - 9.9736\bar{h}^3 + 20.2948\bar{h}^4 - 33.0351\bar{h}^5 + 47.1063\bar{h}^6 - 40.7555\bar{h}^7 + 19.678\bar{h}^8), \quad (\text{A.5})$$

where ν is Poisson's ratio.

- With $\bar{h} \in [0, 0.6]$:

$$C(\bar{h}) = 2 \left(\frac{\bar{h}}{1 - \bar{h}} \right)^2 (5.93 - 19.69\bar{h} + 37.14\bar{h}^2 - 35.84\bar{h}^3 + 13.12\bar{h}^4). \quad (\text{A.6})$$

Note that achieving a ratio between the depth of the crack and the height of the beam (\bar{h}) up to 0.9 is not realistic. However, the beam studied in this paper is assumed to be made of reinforced concrete. Therefore, even if cracking occurs in a ratio of 0.9, the steel component remains connected to the beam. Furthermore, the analysis provides a formulation to calculate the stiffness of the massless rotational springs, as shown in Eqs. (A.5) and (A.6).

When the beam experiences an external force, there is a discontinuity in the slope of the deflection at the crack position. As a result, Green's function is not smooth, and we need to separate it at each crack position as follows:

$$G(x, \omega, a) = \begin{cases} A_1 e^{\lambda x} + B_1 e^{-\lambda x} + A_2 e^{j\lambda x} + A_4 e^{-j\lambda x}, & \forall x \in [0, x_c] \\ \dots \\ C_j e^{\lambda x} + C_j e^{-\lambda x} + C_j e^{i\lambda x} + C_j e^{-\lambda x}, & \forall x \in [x_c, x_{c+1}] \\ \dots \\ C_n e^{\lambda x} + C_n e^{-\lambda x} + C_n e^{i\lambda x} + C_n e^{-\lambda x}, & \forall x \in [x_c, a] \\ B_1 e^{\lambda x} + B_2 e^{-\lambda x} + B_1 e^{i\lambda x} + B_2 e^{-\lambda x}, & \forall x \in [a, L] \end{cases}$$

At the crack position j , the condition of the beam can be presented as follows:

- Continuity of displacement, moment and shear force at $x = x_{c_j}$:

$$\begin{cases} G(x_{c_j}^+, \omega; a) - G(x_{c_j}^-, \omega; a) = 0, \\ \frac{\partial^2 G(x_{c_j}^+, \omega; a)}{\partial x^2} - \frac{\partial^2 G(x_{c_j}^-, \omega; a)}{\partial x^2} = 0, \\ \frac{\partial^3 G(x_{c_j}^+, \omega; a)}{\partial x^3} - \frac{\partial^3 G(x_{c_j}^-, \omega; a)}{\partial x^3} = 0. \end{cases}$$

- Discontinuity of slope at $x = x_{c_j}$ can be found as follows:

$$\frac{\partial G(x_{c_j}^+, \omega; a)}{\partial x} - \frac{\partial G(x_{c_j}^-, \omega; a)}{\partial x} = \frac{E_s I_s}{k_e} \frac{\partial^2 G(x_{c_j}^+, \omega; a)}{\partial x^2}.$$

There are four equations associated with each crack, depending on both the position and depth of the crack. Consequently, there are $4n$ equations for n cracks. In addition, there are eight equations tied to the boundary conditions and the moving loads. Finally, the $4(n+2)$ unknowns can be determined analytically or numerically using the $4(n+2)$ boundary conditions of the problem.

Hence, leveraging the information on the moving loads $R(x, t)$, the dynamic responses of the beam on the scholastic foundation in the frequency domain are delineated in Eq. (5). These responses are subsequently converted back into the time domain using the inverse Fourier transform. In the following section, this result will be used to construct a dynamic model of a railway sleeper.